geologica acta

Citation: Gomez-Ortiz, D., Martín-Velázquez, S., Martín-Crespo, T., Rodríguez-Santalla, I., de Ignacio-San José, C., 3 Martínez-Pagán, P., Martínez-Segura, M., 2025. Electrical resistivity imaging to monitor water infiltration and contamination risk assessment in tailings ponds. Geologica Acta, 23.30, 1-pgs. DOI: 10.1344/GeologicaActa2025.23.30 Online ISSN: 1696-5728

Electrical resistivity imaging to monitor water infiltration and contamination risk assessment in tailings ponds

David Gomez-Ortiz[1,2] Silvia Martín-Velázquez[1,2] Tomás Martín-Crespo[1,2,*] Inmaculada Rodríguez-Santalla[1,2] Cristina de Ignacio-San José[2,3] P. Martínez-Pagán[4] Marcos Martínez-Segura[4]

[1]Departamento de Biología, Geología, Física y Química Inorgánica, Escuela Superior de Ciencias Experimentales y Tecnología, Universidad Rey Juan Carlos

C/Tulipán s/n, Móstoles, 28933 Madrid, Spain; Gomez-Ortiz E-mail: david.gomez@urjc.es; Martín-Velázquez E-mail: silvia.martin@urjc.es; Martín-Crespo E-mail: tomas.martin@urjc.es; Rodríguez-Santalla E-mail: inmaculada.rodriguez@urjc.es

[2]Research Group in Environmental Geophysics and Geochemistry, Universidad Rey Juan Carlos

C/Tulipán s/n, Móstoles, 28933 Madrid, Spain

[3]Departamento de Mineralogía y Petrología, Facultad de Ciencias Geológicas, Universidad Complutense de Madrid

C/José Antonio Novais, 12, 28040 Madrid, Spain; de Ignacio-San José E-mail: cris@geo.ucm.es

[4]Departamento de Ingeniería Minera y Civil, Escuela Técnica Superior Ingeniería de Caminos, Canales y Puertos y de Ingeniería de Minas, Universidad Politécnica de Cartagena

Paseo Alfonso XIII, 52, 30203 Cartagena, Spain; Martínez-Pagán E-mail: p.martinez@upct.es; Martínez-Segura E-mail: marcos.martinez@upct.es

*Corresponding author

ABSTRACT

This study investigates the internal structure and water content variations of the abandoned tailings ponds in the Hiendelaencina Ag-mining district, Spain, using Electrical Resistivity Imaging (ERI). The objectives were to delineate the geometry of the tailings deposits and to assess the spatial and temporal changes in water content within the ponds and the underlying geological units. The pollution risk assessment was evaluated as well. Six resistivity profiles were obtained during two separate field campaigns in September 2020 and May 2021, allowing for a comparison of resistivity data under different moisture conditions.

The results revealed three distinct resistivity zones corresponding to the tailings, Cenozoic sedimentary deposits, and the underlying metamorphic basement, respectively. Temporal variations in resistivity indicates significant changes in water content between the two field campaigns, with increased water infiltration following spring rainfall. While no direct soil moisture measurements were available for calibration, the ERI results provide robust qualitative insights into relative water content changes and infiltration pathways.

Notably, the fractured metamorphic basement showed higher water saturation, indicating vertical and lateral water flow from the tailings. These findings suggest that the tailings ponds are not impermeable, with water infiltrating into deeper layers, potentially transferring pollutants into the groundwater system. The study highlights the effectiveness of ERI as a non-invasive tool for investigating mining sites and provides important insights into the hydrological behavior of mine tailings, which is critical for environmental monitoring and risk assessment.

KEYWORDS **Tailings ponds; electrical resistivity imaging; water content variations; environmental monitoring; Hiendelaencina (Guadalajara)**

INTRODUCTION

Mining of metalliferous mineral deposits and the associated smelting and metal processing activities have had significant impacts on surface environments (Dudka and Adriano, 1997; Žibret *et al.*, 2018). These activities involve the extraction of valuable metals from ores, resulting in the generation of substantial quantities of mine tailings, which are essentially watery sludges containing medium- to fine-grained materials (*e.g.* Kossoff *et al.*, 2014; Martín-Crespo *et al.*, 2019; Martínez-Pagán *et al.*, 2021). The composition of these tailings typically includes a variety of metals and other potentially harmful substances. Over time, the tailings undergo natural leaching, with the reactive materials within them releasing contaminants into the surrounding environment, leading to environmental pollution in the vicinity of the deposits (Dold, 2014; Gómez-Ortiz *et al.*, 2010; Olías *et al.*, 2016, among others).

Consequently, mining and processing of metalliferous mineral deposits have resulted in disturbances of the surface environment, primarily due to the stacking of mine tailings and subsequent mobilization of pollutants into the surrounding environmental compartments. The release of contaminants from mine tailings can have far-reaching consequences for ecosystems and human health. Heavy metals, such as arsenic, cadmium, copper, and lead, are commonly found in tailings and can pose serious risks to wildlife and human populations (Alengebawy *et al.*, 2021; Meza-Figueroa *et al.*, 2009; Vásquez *et al.*, 2015). When these contaminants leach into nearby soil and water bodies, they can accumulate in the food chain, potentially causing long-term harm to plants, animals, and humans through bioaccumulation and biomagnification processes (Cacciuttolo *et al.*, 2023; De Araújo *et al.*, 2022; Lindsay *et al.*, 2015). The risks associated with abandoned hazardous deposits are heightened due to the uncontrolled dispersion and mobilization processes, posing significant threats to the environment. Therefore, the characterization and management of these hazardous materials become crucial.

The Hiendelaencina mining district, located in the province of Guadalajara (Spain), is a notable example of abandoned mining waste. With a rich mining heritage, this district was primarily focused on the extraction and processing of Ag-bearing minerals (López Gómez, 1969). The silver deposit is composed of several veins, which can be grouped by their relative age, mineralization, and/or orientation. The most relevant among them is the Rico vein which, according to research carried out by the Spanish Geological and Mining Institute IGME (1972), has a total exploited length of 1,600m, with roughly 700 additional meters still unexploited to the west. It has an average N70°E trend and a variable dip between 85°S and 75°N (Portero *et al.*, 1982). Silver was mainly obtained through the metallurgical treatment of ores found in polymetallic hydrothermal Zn-Pb-(Cu-Ag) deposits (Martínez-Frías, 1992). Hiendelaencina stands out not only for its paragenesis but also for the presence of specific silver minerals such as dyscrasite (Ag_3Sb), silver halides, and native silver, which contribute to its high silver grade (Calvo and Sevillano, 1992; López Gómez, 1969). Mining operations spanned from the late 19th century, when the first silver vein was discovered, to the early 21st century, when the old tailings were reworked (Calvo and Sevillano, 1992; de Pablo *et al.*, 2013).

The metallurgical treatment of these materials resulted in the production of a large quantity of fine sludges, which were stored in two adjacent slurry ponds near the village of Hiendelaencina, specifically the San Carlos mine ponds (Fig. 1). Previous studies have examined the mineralogical and geochemical characteristics of these sludges, and conducted geomorphological mapping of the ponds to determine the total volume of stored pollutant elements and their erosion rate (Martín-Velazquez *et al.*, 2022; Martín-Crespo *et al.*, 2023). However, there is currently insufficient information regarding the internal structure and condition of the mine pond, spatial variations of the fine sludges, and the potential interconnections between the water stored in the pond and in surface and groundwater outlets. To address these knowledge gaps, a non-destructive method was required to investigate the deposit without disturbing its potentially hazardous contents. Among the various geophysical methods available, we have opted for Electrical Resistivity Imaging (ERI) due to its extensive utilization in recent years for a wide range of geological and environmental applications (Loke *et al.*, 2013; Reynolds, 2011). The use of ERI for the characterization of mine deposits has considerably increased during the last years, and many examples of its different applications, such as acid mine drainage, dam instability, internal structure and physicochemical characterization are available from the literature (see Martínez-Pagán *et al.*, 2021 and reference therein).

The primary objective of this study is gaining insight into the internal structure of the abandoned mine ponds by means of ERI. This geophysical method will also enable the investigation of spatial and temporal variations in water distribution within the pond. The combination of these parameters with the results from the geophysical analysis will provide clarity on the presence of potential transfer of acid mine drainage and/or dissolved pollutants between the mine ponds and the surrounding environment.

STUDY AREA

Geological, hydrological and climatological context

The mining district of Hiendelaencina, along with its homonymous municipality in northern Guadalajara

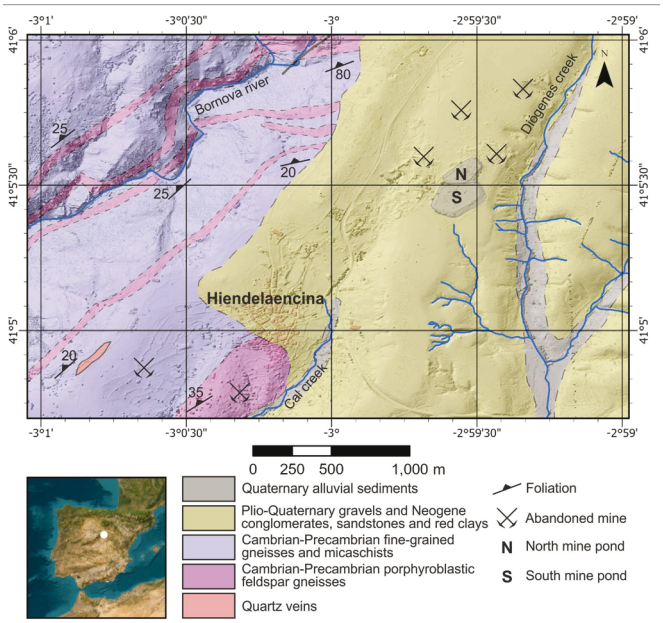

FIGURE 1. Geological map of the study area overlaid on a digital elevation model, showing the location of the Hiendelaencina mining district within the Iberian Peninsula. The geological map is modified from Portero *et al.* (1982), and the digital elevation model is derived from the 2014 LiDAR survey (IGN, 2021).

province, Spain, is situated on a plain at an altitude of 1,085meters between the Alto Rey and Bodera mountain ranges (Fig. 1). It lies in the northeastern region of the Spanish Central System, within the Centro-Iberian zone of the Variscan Massif (Concha *et al.*, 1992). The materials comprising the area span geological times from the Precambrian (metamorphic rocks) to the Quaternary (alluvial materials near stream and river channels) (Portero *et al.*, 1982). The Precambrian metamorphic materials, correspond to the "Ollo de Sapo" glandular gneisses micaschists and quartzites, which are unconformably overlain either by Mesozoic detrital sedimentary materials or by Neogene conglomerates, sandstones, and clays. All these units are in turn overlain by a thin unit of Plio-Quaternary gravels and sands known as "raña," which constitutes the plain on which the mine tailings were deposited (IGME, 1999a,b) (Fig. 1).

This region is located in the Bornova River basin, a tributary of the Henares River, belonging to the hydrographic basin of the Tajo River, one of the most important drainage basins in Spain. The lowest point in the municipality is where the Bornova River is dammed in the Alcorlo reservoir for irrigation and water supply, although the main water supply for Hiendelaencina comes from springs. The population center is located between the channels of two creeks or seasonal streams: La Cal and Diógenes (Fig. 1).

The nearest climatological station to Hiendelaencina is 30km to the east in the Sigüenza village (State Meteorological Agency AEMET: station code 3130C). The normal climatic values for the period between 1985 and 2010 are as follows (Belén and de Pablo, 2016): the average minimum and maximum temperatures are around 5°C and 15°C respectively; the average annual temperature ranges between 10-12.5°C, and the average annual accumulated precipitation is approximately 550mm. Figure 2 shows temperature and precipitation data during the time span of the geophysical surveys. According to the Köppen classification, the climate is Csa, a temperate climate characterized by dry and hot summers with scarce precipitation in winter (Belén and de Pablo, 2016). In this area of the Iberian Peninsula center, the climate is also of continental type.

Abandoned mine tailings

The two mine ponds of San Carlos are located just 1.5km northeast of the Hiendelaencina village. They have an active drainage system that allows them to achieve high compaction and mechanical stability, and their sludges are of medium grain size (Fig. 3A). The pond growing method was based on the slurry discharging by gravity from wooden sluices located right along the border of the storage area (Martínez-Pagán *et al.*, 2021). A dam was not necessary using this tailings pond growing methodology. A slightly crest is delineated at the northwest of the N pond and the main downstream slope at the SSE, leading to an ephemeral lagoon at the S pond center. Foundation structures have not been implemented and drainage channels still can be observed at the slope of both ponds. The discharge system associated with this methodology can be observed in Martín-Crespo *et al.*

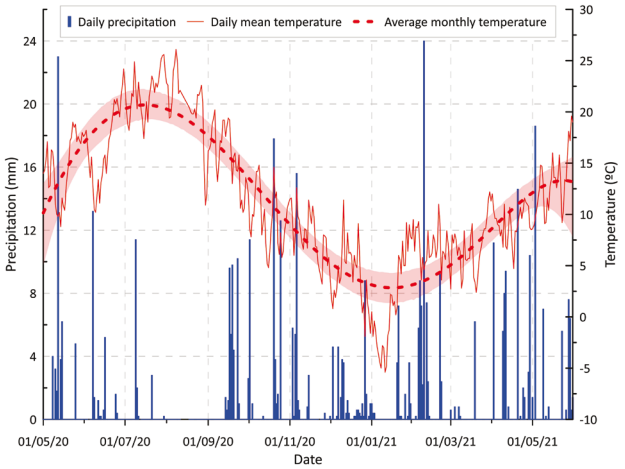

FIGURE 2. Temperature and precipitation data recorded at the Sigüenza meteorological station (AEMET, 2022), representing climatic conditions during the study period.

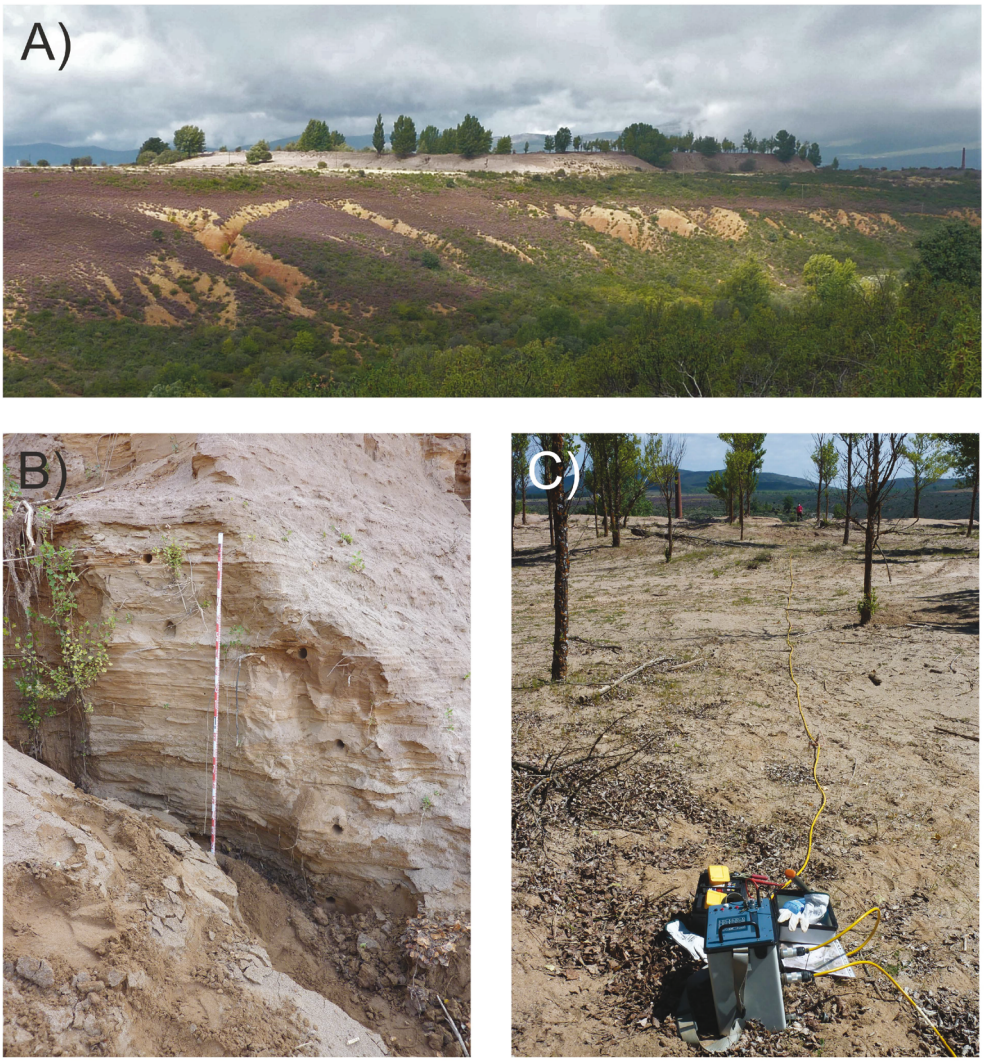

FIGURE 3. Field features of the study area. A) Southwest view of the San Carlos mine ponds overlying Cenozoic materials in the Diógenes Valley. B) Detail of the mine tailings deposits and sample collection. C) Picture of the geophysical survey during data acquisition.

(2023), and the complete geomorphological study were carried out in Martín-Velázquez (2022). An approximate length of 400m and a height of 12m have been measured, resulting in an estimated volume of sludge of 300,000m^3 of sludge in the north pond and 330,000m^3 in the south pond (Martín-Velázquez *et al.*, 2022). According to the USDA textural classification, these authors have also calculated the grain size of the sludge from loamy sand to sandy loam (Fig. 3B).

The deposits have quite a similar composition: quartz (40-60wt%), muscovite (20-30wt%), feldspars (5-15wt%), siderite (5-10wt%) and barite (5wt%) (Martín-Crespo *et al.*, 2023). The presence of quartz, feldspars and muscovite in significant quantities is clearly reflecting the mineralogy of the gneissic host-rock of the mineralization. Other gangue minerals such as siderite and barite, as well as ore minerals (*e.g.* pyrargyrite) have also been identified.

The 11 most significant elements in terms of potential toxicity were analyzed in both ponds: Ag, As, Ba, Cr, Cu, Fe_2O_{3total}, Ni, Pb, S, Sb and Zn (Martín-Crespo *et al.*, 2023). Ba and Fe_2O_{3total} show significantly high contents, up to 10wt% and 8wt% respectively, related to the presence of paragenetic barite and Fe-carbonates and sulfides. Concentrations obtained for the rest of minor and trace elements are those expected in this type of mining slurries: 4-38mg/g for Ag, 20-500mg/g for As, 20-100mg/g for Cr, 8-150mg/g for Cu, 12-22mg/g for Ni, 36-1410mg/g for Pb, 0.1-0.3wt% for S, 8-123mg/g for Sb, 80-560mg/g for Zn. In relation to the element distribution with depth, the north pond exhibits higher contents in almost all the elements at

two depth levels, between 2-3m and between 7-9.5m. In the south pond, only Cu, Fe Pb and Sb seems to increase their concentration at around 3.5m depth. All the slurry samples show alkaline pHs values, most of them having a pH>8, and acid drainage leachate was not observed at any point along the pond contour (Martín-Crespo *et al.*, 2023).

METHODOLOGY

Several ERI profiles were carried out on both slurry ponds in two orthogonal orientations (Fig. 3C). In addition, field samples of the slurry materials were collected to obtain physicochemical parameters that help to interpretate the resistivity data.

Electrical Resistivity Imaging (ERI)

ERI is a widely used geophysical technique for subsurface characterization and imaging (Loke *et al.*, 2013; Reynolds, 2011). It is based on the measurement of electrical resistivity, which is the inherent property of materials to resist the flow of electric current. ERI provides valuable information about subsurface geology, groundwater flow, and contaminant distribution. This method works by injecting electric current into the ground through electrodes and measuring the resulting differences in electric potential.

The principle behind ERI is that different materials have different electrical resistivities. For example, highly resistive materials such as dry sand or rock have high resistivity values, whereas conductive materials like clay or water have lower resistivity values. By mapping the spatial variations in resistivity, ERI can delineate subsurface structures and identify geological features such as bedrock, fractures, and groundwater zones (*e.g.* Chambers *et al.*, 2010; Daily *et al.*, 1992; Loke, 2011; Slater and Binley, 2003, among others). One of the key advantages of ERI is its non-invasive nature, allowing for subsurface imaging without the need for drilling or excavation. This makes it a valuable tool for environmental studies, geotechnical investigations, and hydrogeological assessments.

Several techniques are commonly used in ERI surveys, such as the Wenner array, dipole-dipole array, and pole-dipole array, each of which has its own advantages and limitations (Loke, 2011; Loke *et al.*, 2013). The choice of array configuration depends on the specific objectives of the survey and the expected subsurface conditions. Inversion algorithms were used to interpret the resistivity data obtained from ERI surveys (Loke *et al.*, 2013). These algorithms use mathematical models and computational techniques to estimate the subsurface resistivity distribution based on the measured data. Various inversion methods exist, including smoothness-constrained, Occam, and least-squares algorithms, each with its own strengths and limitations.

Both a Syscal Junior Switch 48 (Iris Instruments; Fig. 3C) and a SuperSting R8 (Advanced Geosciences, Inc.) resistivity meters were used and three ERI profiles were surveyed in two different seasons (September 2020 and May 2021). For the subsurface electrical resistivity measurements, a Dipole–Dipole array was used. This configuration was selected because it provides sufficient depth of penetration and is particularly sensitive to lateral variations with depth, which makes it favorable for detecting boundaries and heterogeneities in non-homogeneous regions such as mine tailings deposits (*e.g.* Martínez-Pagán *et al.*, 2021). This sensitivity to lateral heterogeneity was essential for achieving the objectives of our study, namely to delineate boundaries between units and track infiltration pathways. The length of the profiles ranged from 355m (transverse profiles) to 475m (longitudinal profiles), with 5 m of electrode spacing and a maximum investigation depth of ~45m at the central part of the profiles (Bernard, 2003). A Magellan MobileMapper CX differential GPS with submetrical accuracy was used to geolocate the profiles.

Prior to inversion modeling, the data processing involves several steps. First, bad data points are removed by filtering the raw data based on low signal ($V/I < 10{-}6\Omega$) or repeatability errors exceeding 2%. Additionally, topography data along the profile are included. The L1 norm is used for data misfit in each dataset of the profiles, and the inversion process employs the L1 norm (robust) for the model roughness filter, following the method proposed by Loke *et al.* (2013). The robust inversion method is particularly effective in handling sharp boundaries within the model and is employed in all inversions. The inversion method utilizes a finite element scheme to solve the 2-D forward problem and the blocky inversion method to invert the Electrical Resistivity Tomography (ERT) data. By minimizing the smoothing effect on the resistivity data during modeling, the robust inversion method reduces any uncertainties associated with the interpretation and estimation of resistivity models resulting from data smoothing. The decision to use the L1 norm is based on its robustness to outliers, as it minimises the sum of absolute deviations and is therefore less sensitive to outliers in the data. Therefore, it can produce more stable and reliable subsurface models, which is crucial when analysing infiltration phenomena in mining deposits associate with sharper contrast between the resistivity values of the waste body and the host medium giving better contrast that the smoothness-constrained least-squares (L2-norm) as it has been demonstrated by several studies about the effectiveness of this approach, including those by Martínez-Pagán *et al.* (2021), Ibraheem *et al.* (2015) and Liu *et al.* (2020), which address complex

groundwater flow patterns. To ensure the quality and reliability of the inversion results, the absolute root mean square error between the measured and predicted apparent resistivity is monitored. Additionally, the predicted values are compared with the actual field measurements of the mine pond thickness, which typically ranges from 10 to 12 meters.

Computation of water content variations

Archie's Law is a fundamental principle in geophysics that establishes a relationship between the electrical resistivity of a porous medium and the saturation of fluids within it. The modified version of Archie's Law (Archie, 1942) extends this relationship to account for variations in porosity, cementation, and fluid saturation. The equation is expressed as:

$$R_t = a \cdot \varnothing^{-m} \cdot R_w \cdot S_w^{-n} \quad (1)$$

where:

- R_t represents the total resistivity of the medium.

- a is a constant that accounts for rock and fluid properties.

- Ø denotes the porosity of the medium, representing the volume fraction of pore space.

- m is the cementation exponent, indicating the degree of cementation or consolidation of the rock.

- R_w corresponds to the resistivity of the saturating fluid, typically water.

- S_w represents water saturation.

- n is the saturation exponent, reflecting how the electrical resistivity of a porous medium changes as the fluid saturation changes.

- a, m and n are constants specific to the geological medium that can be determined empirically.

To compute the variations in water content (ΔS_w), we employ Archie's modified expression. By comparing the total resistivity (R_t) measured at different times or locations, we can infer changes in water saturation within the subsurface medium.

The computation involves deriving the expressions for for two distinct conditions or time periods, denoted as R_{t1} and R_{t2}. These equations are:

$$R_{t1} = a \cdot \varnothing^{-m} \cdot R_w \cdot S_{w1}^{-n} \quad (2)$$

$$R_{t2} = a \cdot \varnothing^{-m} \cdot R_w \cdot S_{w2}^{-n} \quad (3)$$

Where S_{w1} and S_{w2} are the water saturations corresponding to R_{t1} and R_{t2} respectively.

We subtract equation (2) from (3) to find the difference between S_{w2} and S_{w1}:

$$R_{t2} - R_{t1} = a \cdot \varnothing^{-m} \cdot R_w \cdot S_{w2}^{-n} - a \cdot \varnothing^{-m} \cdot R_w \cdot S_{w1}^{-n} \quad (4)$$

We factor out the common terms:

$$R_{t2} - R_{t1} = a \cdot \varnothing^{-m} \cdot R_w \cdot \left[\left(S_{w2}\right)^{-n} - \left(S_{w1}\right)^{-n} \right] \quad (5)$$

And finally, to express the difference between S_{w2} and S_{w1} as a function of R_{t2}, R_{t1}, a, m and n, we simply isolate $S_{w2}-S_{w1}$:

$$S_{w2} - S_{w1} = \left(\frac{R_{t2} - R_{t1}}{a \cdot \varnothing^{-m} \cdot R_w} \right)^{\frac{-1}{n}} \quad (6)$$

By assuming that the porosity of the material Ø does not change through time and that the resistivity of the saturating fluid R_w is the same, equation (6), which computes the variation in water saturation (ΔS_w) can be simplified to:

$$\Delta S_w = S_{w2} - S_{w1} = \left(\frac{R_{t2} - R_{t1}}{a} \right)^{\frac{-1}{n}} \quad (7)$$

This method enables the quantification of water content variation from electrical resistivity data, facilitating the interpretation of subsurface fluid dynamics and hydrogeological processes. No direct soil moisture measurements (*e.g.* TDR, gravimetric samples, or borehole data) were collected during the surveys due to logistical constraints, and therefore the ERI-derived water content estimates are interpreted qualitatively rather than quantitatively. The water content variations can provide useful information about the hydrological and geophysical properties of the medium, such as the fluid flow, the permeability and the compressibility (Bai *et al.*, 2022; Jiang *et al.*, 2021; Kirkby and Heinson, 2017; Rekapalli *et al.*, 2015; Senger *et al.*, 2021; Whitman and Yeboah-Forson, 2015). They can also be used to monitor changes in the medium due to natural or anthropogenic factors, such as rainfall, drought, irrigation, injection, extraction, or deformation (*e.g.* Brillante *et al.*, 2015; Rao *et al.*, 2020; Vanella *et al.*, 2021). Finally, the water content variations can also be used to detect and characterize the anomalies or features in the medium, such as fractures, faults, cavities, or inclusions (Lee *et al.*, 2021; Liu *et al.*, 2020).

Sampling and analysis

In order to obtain the chemical composition of water leachates from the mine ponds, two samples were collected during the same two geophysical surveys campaigns, September 2020 and May 2021, at an underground water catchment gallery (GAL) dug in the Cenozoic materials just underlying the mine ponds. The pH values were obtained by a multiparametric HANNA Instruments probe before storing refrigerated in 0.5 l volume canister. They were suitably acidified to avoid arsenic methylation. The chemical analyses were performed at the Centro de Apoyo a la Investigación de Ciencias de la Tierra y Arqueometría from the Complutense University of Madrid (Spain). Sampling location were georeferenced using the same GPS device employed for the resistivity profiles.

RESULTS

Geophysical surveys

To obtain information about temporal resistivity variations of the mine ponds related to different humidity conditions inside the deposits, two different field surveys were carried out (Fig. 4). The first survey was conducted at the beginning of autumn (September 2020), just after a ~3-month dry period conditions during the summer. The second survey was conducted at the end of spring (May 2021), following the period of intense rainfall is characteristic of this season (Fig. 2). During both surveys, three ERI profiles were obtained to get a complete covering of the north and south mine ponds. Two of the profiles follow a W-E trend and are transverse to the mine ponds (H1 north pond, H3 south pond), whereas the third one (H2), trending N-S, is longitudinal to the mine ponds and crosses the transversal H1 and H3 profiles at a right angle. To compare results obtained at different times of the year, and under varying moisture conditions, the same profile locations were used in both campaigns. However, in the 2021 field campaign and based on the results obtained in the previous campaign, the length of profiles H2 and H3 was increased to reach a greater depth.

Figure 4 shows the comparison of the 2D electrical sections of the three ERI profiles (H1, H2 and H3) obtained during dry (September 2020) and wet (May 2021) periods for easy evaluation. The upper profile corresponds to the 2020 survey and the lower one corresponds to the same profile but for the 2021 survey. The same resistivity scale has been used for all the profiles, so the colour variations correspond to true resistivity variations between the two different periods considered.

Profiles H1, transverse to the mine north pond, have a maximum length of 275m (autumn 2020). The absolute error during the inversion process, achieved at the fifth inversion, ranges from 4.8% (spring 2021) to 7.3% (autumn 2020). The profiles display the highest resistivity values (>200ohm·m) in both the upper and lower zones, while the central part has intermediate to low resistivity values (<200ohm·m). Three main units with different resistivity values can be observed: i) an upper unit corresponding to the ~12m high mine tailings, with resistivity values ranging from 5 to >1000ohm·m, ii) an intermediate unit ~20-25m thick, with resistivity values ranging from ~5 to 200ohm·m, in which the lower resistivity values are below the tailings but have a greater lateral extent and reach greater depth in the September 2020 profile compared to the May 2021 profile and iii) a lower unit with higher resistivity values in autumn 2020 compared to spring 2021 (>200ohm·m vs. ~100ohm·m, respectively). The boundary between the upper and intermediate units correspond to the topographical surface and is approximately horizontal (Fig. 4). On the other hand, the boundary between the intermediate and lower units, which is slightly undulating as seen in the autumn 2020 profile, is at ~20-25m depth. However, this boundary is barely visible in the spring 2021 profile, as both the intermediate and lower units display similar resistivity values.

Profiles H3, transverse to the mine south mine pond, have a maximum length of 355m (spring 2021). The absolute error during the inversion process, obtained at the fifth inversion, ranges from 5.2% (spring 2021) to 6.4% (autumn 2020). The profiles show a similar resistivity distribution as in H1, with the same three units and boundaries between them previously described. The main difference corresponds to a sub vertical low resistivity zone (<20ohm·m), which appears in the central part of the autumn 2020 profile at the intersection with profile H2. The low resistivity zone has a width of ~30m and extends through both the intermediate and lower zones. Interestingly, this zone is not imaged on the same profile corresponding to spring 2021, although a zone of homogeneous intermediate resistivity values (~100ohm·m) is identified (Fig. 4).

Profiles H2, longitudinal to both north and south ponds, have a maximum length of 475m (spring 2021). The absolute error during the inversion process, achieved at the fifth inversion, ranges from 7.9% (autumn 2020) to 8.2% (spring 2021). The profiles show a similar trend of resistivity, with the three units (upper, intermediate and lower) well defined and with similar characteristics than for profiles H1 and H3. In relation to the depth and geometry of the boundaries between units, although they are similar to previous profiles, the lower one is slightly more irregular with several vertical steps. The same subvertical structure of low resistivity defined for profile H3 (autumn 2020) is imaged in the corresponding intersection point between profiles H2 and H3. However, its width is

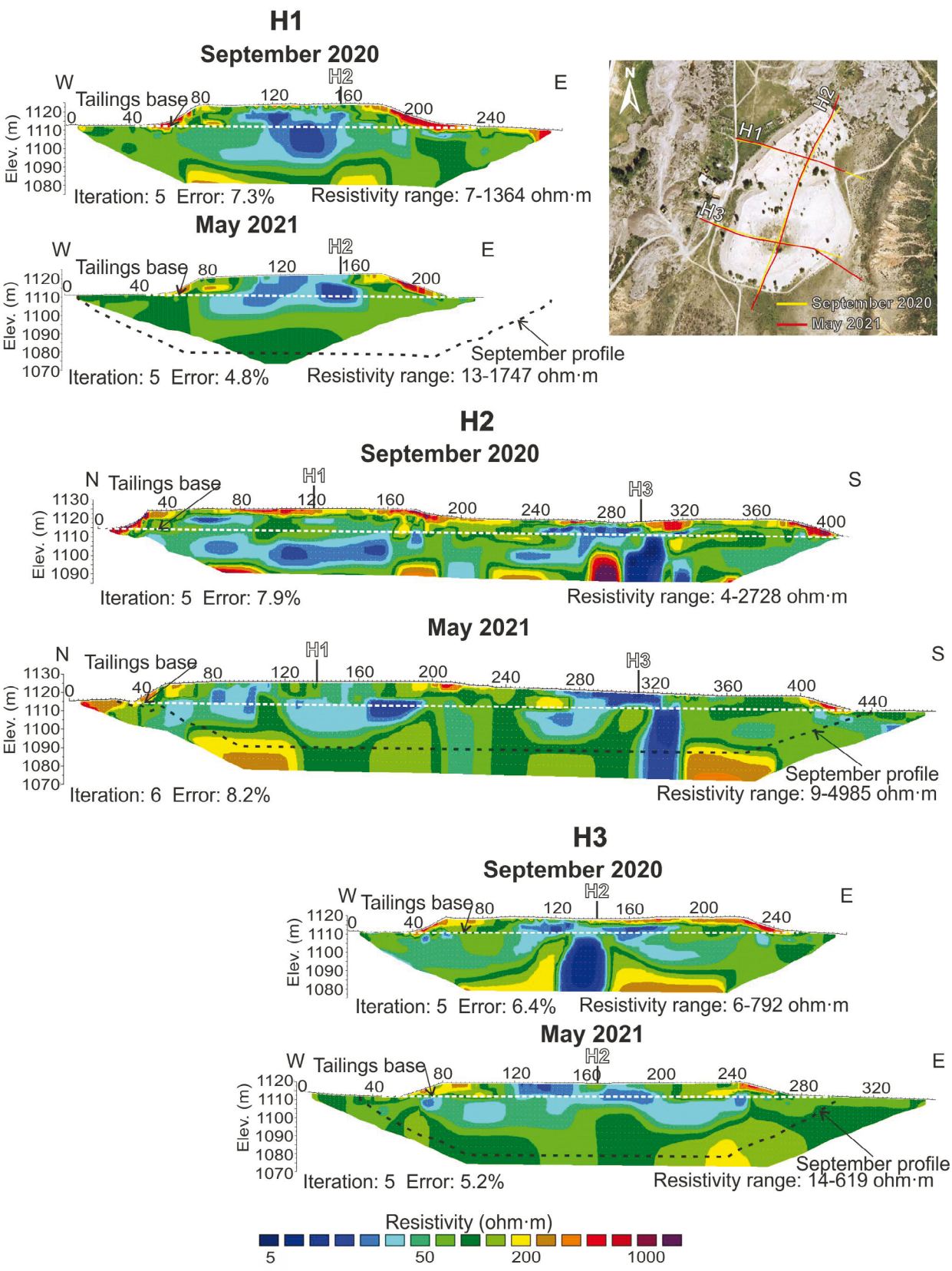

FIGURE 4. Electrical resistivity profiles acquired in September 2020 and May 2021. Profile locations are shown on a 2002 orthophoto from the SIGPAC (Geographic Information System for Agricultural Parcels; IGN, 2021).

TABLE 1. Fe and trace elements content, pH and Electrical Conductivity (EC) values in the catchment gallery water samples

Sample	Ag (μg/L)	As (μg/L)	Ba (μg/L)	Cd (μg/L)	Cu (μg/L)	Fe (μg/L)	Ni (μg/L)	Pb (μg/L)	Zn (μg/L)	pH	EC (μS/cm)
Autumn 2020	0.1	0.4	78.4	b.d.	0.5	10	0.3	0.1	24.6	5.8	261
Spring 2021	b.d.	1.8	97.0	0.1	0.6	330	2.3	3.8	8.3	6.5	207

b.d.: below detection

different depending on the time of the year surveyed. In autumn 2020, the low resistivity area extends horizontally for ~40m, whereas in spring 2021 this width is reduced to ~20m (Fig. 4). As a result, this low resistivity zone does not intersect, and is therefore not imaged in profile H3 in spring 2021, as described previously.

Composition of water

In relation to the catchment gallery water samples analysed, the concentration of the potentially hazardous ions increases from autumn 2020 to spring 2021 (Table 1). In both campaigns the concentrations of As, Cd, Cu, Ni, and Pb are below 4mg/L. Zn concentrations are 24.6 and 8.3mg/L in 2020 and 2021 respectively, showing a reverse pattern. The water samples show pH values of 5.8 and 6.5 in 2020 and 2021 respectively, and low electrical conductivity values, below 300mS/cm in both campaigns.

INTERPRETATION AND DISCUSSION OF RESULTS

Mine pond structure

Based on the resistivity values and their temporal variations obtained from the six profiles of the study zone, a geological interpretation has been made to facilitate analysis (Fig. 5).

The upper zone corresponds to the tailings pond, where areas of high resistivity alternate with areas of low resistivity values (from >1000 to ~5ohm·m). The latter are typical of water saturated porous materials such as tailings. The San Carlos mine pond sludges are fine-grained and loamy sand to sandy loam in character (≈80% sand fraction; ≈5% clay fraction). They are mainly composed of gangue minerals: quartz, and aluminum and iron oxides (Martín-Crespo *et al.*, 2023). Therefore, variations in resistivity values are mainly determined by the amount of water in the pores, or more precisely, by the air trapped in them as air is one of the best electrical insulators. The higher the water content in a material, the lower the measured resistivity value. The intermediate zone has values of intermediate resistivity (~40 to 200ohm·m), although with discrete sectors of low resistivity again due to water infilling the corresponding to Plio-Quaternary and Neogene detrital materials. Finally, the lower zone with higher resistivity (>200ohm·m), typical of dry sands or slightly altered metamorphic rocks (*e.g.* Reynolds, 2011), corresponds to the gneissic basement.

The observed temporal variations in resistivity across these three units correspond to changes in water saturation levels due to groundwater flow, as described later. It is worth noting that the lower zone has higher resistivity in all profiles in September 2020 compared to those in May 2021. The most plausible interpretation for the subvertical feature with low resistivity values identified in H2 and H3 profiles is that it corresponds to a highly fractured zone. Its apparent different in width depends on the amount of water available at different times of the year, allowing water to percolate in during wet periods (decreasing the resistivity) but greatly decreasing its water content during the dry season. The resistivity contrast between the upper and intermediate units allows the geometry of the base of the tailings and their thickness to be clearly defined. The three interpreted profiles in Figure 5 clearly show that the base of the tailings ponds is horizontal, coinciding with the sedimentation surface that defines the upper limit of the recent sedimentary deposits, *i.e.* Plio-Quaternary sands and gravels ("raña" unit). Therefore it can be concluded that the tailings were deposited directly over a pre-existing horizontal surface at 1,110m above sea level that was not modified by any excavations or works during the stuffing of the two tailings ponds. This allows us to easily calculate the thickness of the tailing deposits (Fig. 5): a maximum of 15m for the northern pond and 10m for the southern pond.

Spatio-temporal variations in water content

The resistivity values from September 2020 survey are consistent with the prevailing weather conditions at the time (Fig. 2). The field campaign took place immediately after a very dry and hot summer, with almost no rainfall in July (16.6mm) and August (0mm) (AEMET, 2022). As a result, the deeper materials (sedimentary and metamorphic rocks) have high resistivity values because they were completely dry. The resistivity survey coincided with the onset of the autumn rains (43.6mm in September; AEMET, 2022), which are reflected in the

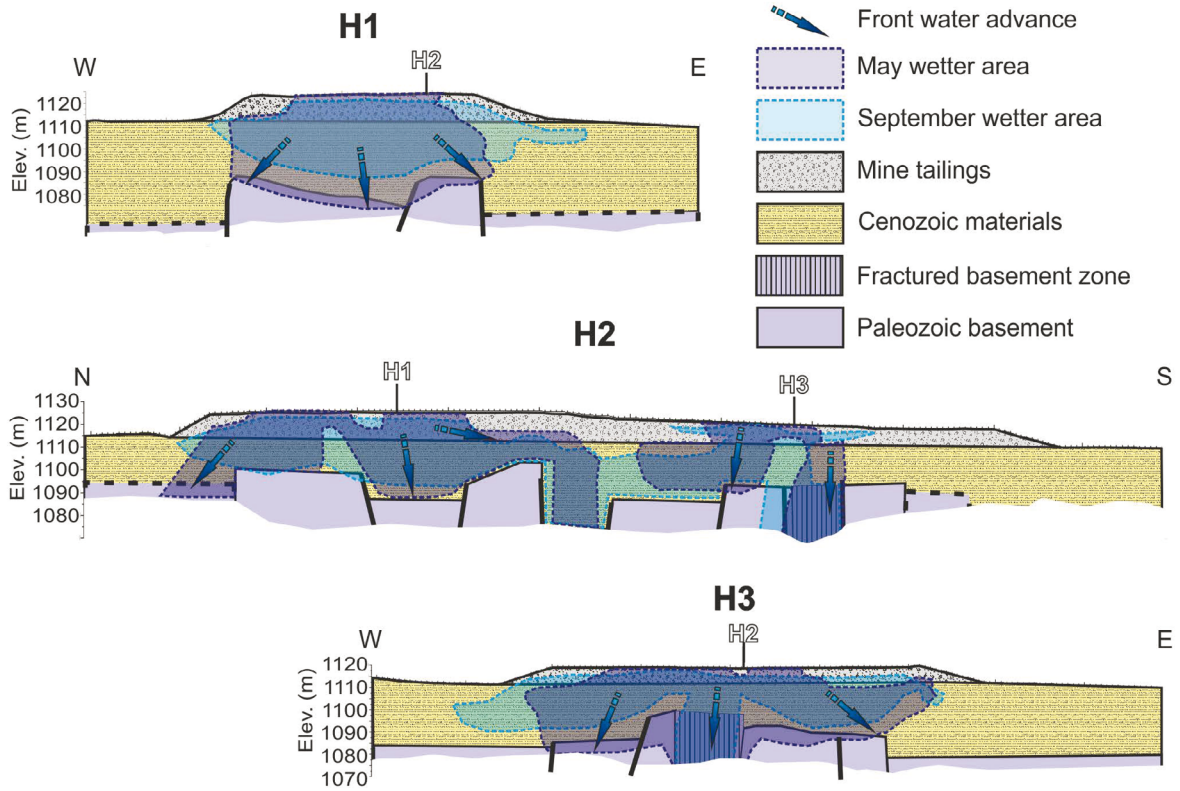

FIGURE 5. Geological interpretation of the resistivity profiles, highlighting the spatial extent of wetter zones identified in the September 2020 and May 2021 surveys.

profiles as low resistivity zones restricted to the upper central part of the ponds. This is due to the progressive infiltration of water, while the edges of the ponds retained high resistivity values due to low water content in these slightly higher topographic areas (Fig. 4-5). At this stage, the basement metamorphic rocks contained water only in highly fractured and therefore more permeable zones (*e.g.* the central area of profile H3). As mentioned above, fractures appear as narrow vertical zones of low resistivity, indicating water flow to deeper areas.

In contrast, during the May 2021 campaign, rainfall had been continuous over the preceding months. From February to April 145mm of precipitation was collected and during the 28 first days of May, 41.8mm were collected (AEMET, 2022). Therefore, the resistivity values obtained in spring are generally lower in all profiles (Fig. 4). The observed reduction in resistivity values in the intermediate and lower units is interpreted as the progressive infiltration of water from the ponds into the sedimentary and metamorphic rocks (Fig. 5). Consequently, the resistivity contrast between them decreases, and some of the low-resistivity fractured zones, which were clearly visible in autumn, become blurred in spring as the resistivity values of fractured and non-fractured areas equalize.

The analysis of the temporal variations in resistivity values has allowed for a quantitative calculation of water content variation (Fig. 6). Given the textural characterization of the tailings deposits, the values of the a and m constants for water saturation calculation were set to 1 and 2, respectively, in accordance with previous studies on detrital sediments (*e.g.* Mohamad and Hamada, 2017). Using the resistivity values from the spring 2021 profiles as a reference, the temporal variation in resistivity, obtained by subtracting the fall 2020 profiles from the Spring 2021 profiles, was converted into water saturation variation expressed in percentage.

In the case of profile H1, the variation in water saturation ranges from -60% to 50% (Fig. 6). Negative values, indicating a loss of water between the two time periods considered, are mainly found in the eastern part of the profile, both in the surface tailings and in the sedimentary and metamorphic rocks. Positive values, indicating an increase in water content, are found in the

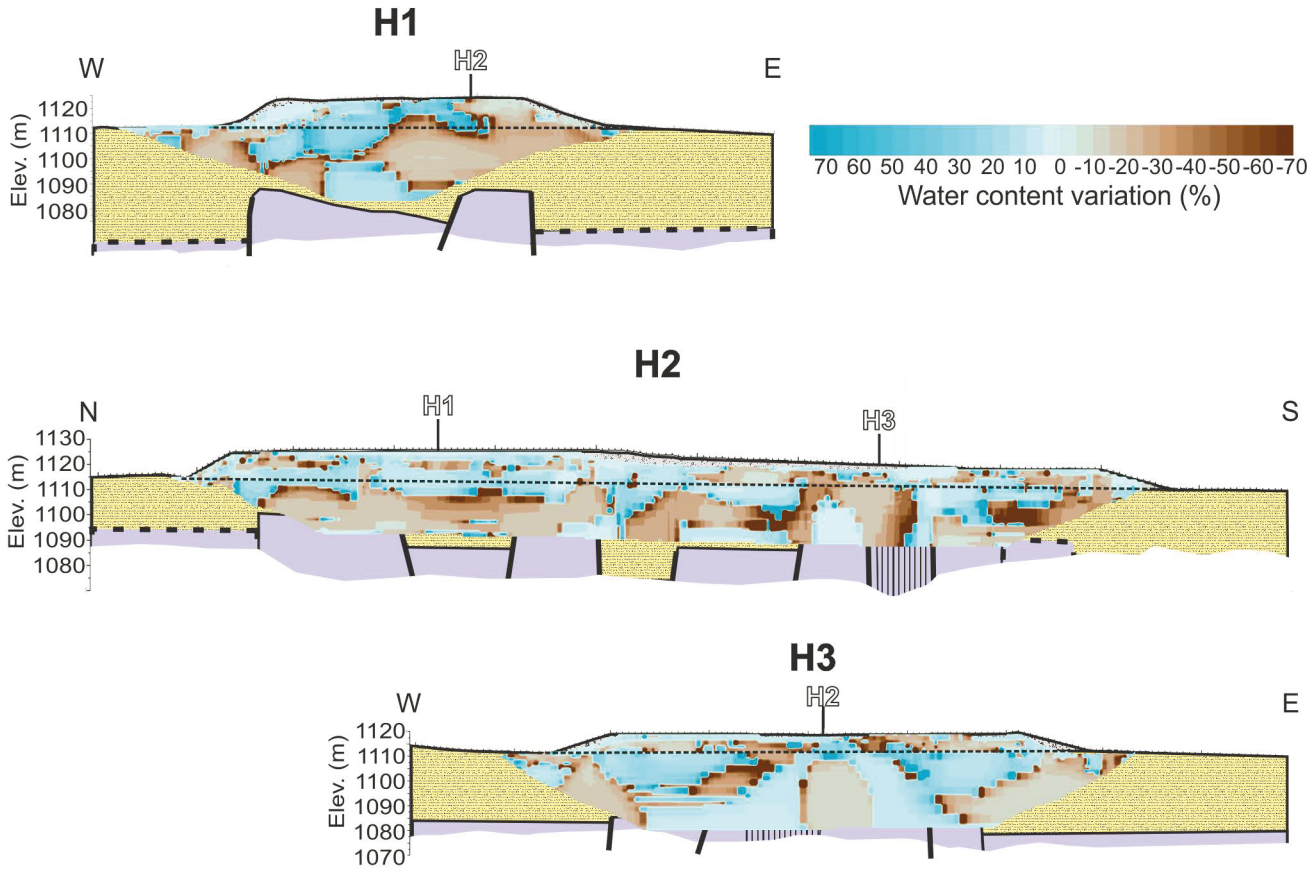

FIGURE 6. Spatial distribution of changes in water content between September 2020 and May 2021, derived from the temporal variation in resistivity measurements.

central part of the profile, in all three differentiated units (tailings, sedimentary, and underlying metamorphic rocks). These variations indicate that between autumn 2020 and spring 2021, water flowed from the more superficial part of the north pond tailings towards the geological units immediately beneath, which were drier at the time. Infiltration occurred both horizontally and vertically, as evidenced by the increase of 10 to 20% water saturation at the western edge of the pond, while the central area of the underlying sedimentary and metamorphic rocks shows an drastic increase in water content of 20 to 50%.

A similar pattern is observed in the south pond (profile H3, Fig. 6), with water content variations ranging from -50% to +50%. Most of the tailings in this pond show negative values, indicating a loss of water to the underlying Cenozoic materials. The latter show the highest increases in water saturation indicating that they were receiving the infiltrated water both laterally and vertically. A notable feature of this profile is the behaviour of the underlying metamorphic rocks. In autumn 2020, they exhibited very high resistivity values, except for a central vertical zone of very low resistivity, interpreted as a fracture zone containing a high amount of water. In spring 2021, this central zone shows a 15% decrease in water content, while the surrounding areas increase it by 10 to 30%. This indicates that during the studied period the water contained in the central fractured zone infiltrated even deeper, while the less fractured surrounding metamorphic rocks increased their water content as they progressively received infiltrated water from both the tailings and the Cenozoic materials.

The longitudinal profile H2 shows water content variations in both tailings ponds simultaneously. Due to the shallower depth of investigation for this profile, as explained in the methodology section, profile H2 primarily shows the water content variations of the two upper units, *i.e.* the tailings deposits and the sediments. Ranging from -70% to +60% over the studied period. Overall, with the exception of the uppermost part of the mining ponds, which show discrete areas of moderate increase in water content, the mine tailings exhibit the greatest decreases in water content, while the Cenozoic materials show the greatest increases in water retained in their surface areas. The boundary between

positive and negative water content variations is clearly located at the contact between these two units, confirming the water infiltration flow pattern observed in the cross sections of H1 and H3 profiles. Finally, and focusing on the mine tailings, a certain difference in the changes of water saturation can also be observed. While the north pond exhibits an increase in water saturation reaching a maximum of 50 to 60% across most of its extent, the south pond shows a more stratified pattern. In its uppermost layer (0 to 4m depth), there is a maximum increase in water content of 40 to 50%, whereas in the deeper layer (4 to 10m depth), a decrease in water content is observed. These differences suggest a variation in the internal structure of the two tailings ponds.

Several studies have used ERI to estimate water content in different contexts, such as landfill imaging (*e.g.* Neyamadpour, 2019), root zone monitoring (*e.g.* Garré *et al.*, 2011), hydrogeological investigations (*e.g.* Dietrich *et al.*, 2014), and irrigation studies (*e.g.* Jayawickreme *et al.*, 2010). For the specific case of determining water content in mine tailings, few studies have combined ERI with the petrophysical properties of mine deposits to obtain reliable water content values (*e.g.* Dimech *et al.*, 2022, 2023; Martínez-Pagán *et al.*, 2021; Mollehuara Canales *et al.*, 2020). In most cases, mine tailings have a high clay content, which makes it difficult to apply Archie's Law directly, as it is designed for non-conductive matrix environments. For example, Mollehuara Canales *et al.* (2020) note that clay minerals significantly effect on electrochemical processes, affecting resistivity measurements. In geologic formations with high clay content, surface conduction can be significant, requiring modifications to Archie's Law. The most used variant is the Waxman-Smits equation (Waxman and Smits, 1968), which relates surface conduction to the Cation Exchange Capacity (CEC) of clay minerals. Other models, such as those of Bussian (1983), and De Lima and Sharma (1990), used a two-component system, while Revil and Glover (1998) expanded this with differential effective medium theory, incorporating pore water composition and electrical double layers. More recently, Revil *et al.* (2018) explained the non-linear behaviour of conductivity in granular materials through salinity effects on pore network and surface conductance. However, the ponds of the Hiendelaencina mine have tailings with minimal clay content, mostly composed of silicate and carbonate minerals. Therefore, our use of a simplified Archie's Law without consideration of surface conductance is valid in this case.

It is noteworthy that no direct soil moisture measurements (*e.g.* TDR probes, gravimetric sampling, or borehole data) were available at the site during the geophysical surveys. Consequently, the water content values derived from ERI must be regarded as qualitative indicators rather than absolute measurements. This limitation is common in field studies, as site-specific calibration is often logistically challenging and can be more time-consuming than the geophysical surveys themselves (*e.g.* Tso *et al.*, 2019). Despite this limitation, the time-lapse approach adopted here provides robust insights into relative changes in moisture content and the dynamics of infiltration. Consistent with results from controlled field experiments (de Jong *et al.*, 2020), the resistivity variations observed between autumn 2020 and spring 2021 delineate infiltration fronts and zones of water redistribution in agreement with precipitation records and the geological setting. Future investigations should aim to complement ERI with in situ moisture measurements to calibrate the resistivity–moisture relationship and to improve the quantitative accuracy of water content estimates.

Temperature variations are known to affect bulk resistivity, with sensitivities of approximately 1.5–2% per °C (Grellier *et al.*, 2006; Hayley *et al.*, 2007; Ma *et al.*, 2011). However, meteorological data show that the mean daily temperature during the autumn 2020 survey was 15°C, while during the spring 2021 survey it was 14°C, yielding only a 1°C difference. This would imply a maximum effect of ~2% on resistivity, which is negligible compared to the much larger variations (up to 50–60%) observed between surveys. Furthermore, temperature variations are expected to be restricted to the shallow active zone, while deeper layers remain largely unaffected (Hermans *et al.*, 2014). We therefore consider that the observed resistivity changes primarily reflect variations in water content rather than temperature effects.

Another important consideration is that the penetration depth of the 2020 profiles H2 and H3 was slightly shallower than that of 2021. This results in reduced resolution in the deepest parts of the 2020 models (approximately the lower 10m). Nevertheless, the main resistivity structures at depth are consistent across both datasets, indicating that their location and geometry are robust. At shallow to intermediate depths, where water inflow from the surface is better resolved, both surveys provide comparable resolution, making temporal comparisons reliable in these zones. Only the deepest features of profiles H2 and H3 should therefore be interpreted with some caution.

In summary, the analysis of spatio-temporal variations in water content indicates the existence of water flow by infiltration from the mining tailings deposits into the sediments, both laterally and in depth, in a generalized manner, without clear preferential flow paths. Once the water reaches the Cenozoic materials, it continues to infiltrate into the lower metamorphic unit, and from there into deeper areas, primarily through more permeable, vertically fractured zones. Therefore, the compounds dissolved in the

water circulating through the ponds will eventually reach the deeper aquifers and consequently surface waters fed by groundwater flows. Metals and semi-metals concentrations in the water samples collected from the catchment gallery dug at the Cenozoic materials immediately underlying the ponds, roughly match the moderate contents of these elements in the mine ponds, proving infiltration is partially feeding this catchment gallery.

Environmental issues and the need for study

Mining activities and extractive metallurgy have undeniable economic and social benefits, but due to the generation of a large amount of waste (solid, liquid, and gaseous), they are strongly linked to a significant environmental risk (Doumas *et al.*, 2018; Jarsjö *et al.*, 2017; Martínez-López *et al.*, 2021; Pashkevich, 2017).

In order to stablish the better criteria for dam security, several tailings dam classification frameworks have been defined at the last decades. These classifications are usually determined by the consequences to infrastructures, cultural and environmental resources, and human life (Rodríguez-Pacheco *et al.*, 2025). The Environmental Consequence Classification (ECC) published by the Canadian Dam Association (CDA, 2024), the Global Industry Standard on Tailings Management (GISTM) by the Global Tailings Review (GISTM, 2020,) and the Consequence Classification published by the International Commission on Large Dams (ICOLD, 2023) are three good examples of dam classifications. The Hiendelaencina tailings ponds are not hazardous tailings dams by two main reasons: the San Carlos tailings ponds were abandoned since 1990s, and they have an active drainage system that allows them to achieve high compaction and mechanical stability. As previously mentioned, a dam was not necessary. Taken into account such good stability conditions, the San Carlos ponds have been classified as Low Category according to their environmental classifications (CDA, 2024; GISTM, 2020; ICOLD, 2023).

Among several possible impacts, water resource pollution stands out: ecosystems, surface water, and groundwater stands out and potentially poses a serious problem for their conservation and subsequent use of the environmental compartments. Currently, research dedicated to the study and solution of this problem is one of the priority scientific activities within the context of mining heritage conservation.

Waters affected by mining activities usually show one or more of the following features: turbidity, acid pH and high concentration of sulfate, Fe, Al, and other metals. The main difference between organic and metal pollution is the fact that the latter cannot be destroyed by biological or chemical processes but only eliminated or reduced by physical processes. The different metals mobility, quantity and distribution are difficult to model and predict, since multiple physicochemical, geological and topographical factors need to be considered, as well as the mining technologies used (Smith, 2007). In the case of this study, the Zn content in the water sample could became alarming. According to Lewis (2010) the solubility of Zn is a function of pH such that it is greatly enhanced at low pH but decreases drastically as pH rises to 7, at which point it is no longer soluble. In the 2020 campaign, with a pH value of 5.8, there is more Zn dissolved in the water, whereas in 2021 with a pH value of 6.5, Zn decreases greatly as it approaches insolubility.

The environmental impact of water discharged from mines and tailings ponds is significant. The study of Martín-Crespo *et al.* (2010) presented the results of a monitoring study carried out at Mina Concepción mine pond (Iberian Pyrite Belt), based on mineralogical, geochemical and geophysical (ERI) techniques. The infilling thickness, as well as variation and geometry of water leakages through the bottom of the pond were characterized. The existence of an internal remnant flow of acidic waters, which tended to escape through the pond dyke, was clearly identified. As warned in the IGME Environmental Impact Assessment Reports (1999a,b), the San Carlos mine slurry ponds have good stability but, as demonstrated in this study, they are not impermeable and a surface water recovery and treatment system would be necessary. Leachate and infiltration water are drained at the bottom, reaching both surface water and groundwater (including the catchment gallery).

In Spain there are no quality levels defined in the legislation for groundwater not intended for human consumption. In order to assess heavy metal pollution the Dutch regulation is normally used as a reference (ESDAT, 2009). This is especially evident in cases of industrial pollution. This regulation has two levels: a target level, which is a quality limit value, and an intervention level, the limit that above which intermediate action is required to remedy the deviation from the standard. The Hiendelaencina tailings contain significant barite and siderite contents (Martín-Crespo *et al.*, 2023). Although leakage from the tailings into the underlying sedimentary and metamorphic rocks was clearly identified by ERI, the pH remains normally neutral becoming only slightly acidic during the rainy season. Mobile elements such as Zn, increase their concentration from dry to rainy period, probably remaining adsorbed onto minerals resulting of siderite alteration, such as Fe oxides/hydroxides (Kucerová *et al.*, 2014). This could explain that the analysed elements in the catchment gallery samples do not exceed the target level.

Apart from the ponds, there are several open shafts in the Hiendelaencina mining district that serve as direct entrances to the flooded mine galleries by groundwater after the completion of the exploitation. The analyses of the water sample collected from the shafts would be very illustrative of the metal and semi-metal pollution. The affected area can extend beyond the mining district itself, and both wind and water transport can be decisive factors in this regard (Martín-Velázquez *et al.*, 2022). Regarding the mining ponds, the fine particle size of the sludge facilitates the remobilization of the material, and when saturated with water, they can behave like a fluid (García García, 2004). Additionally, the decrease in grain size of the sludge is inversely proportional to its degree of exposure to oxidation processes (González, 2011). Hydrogeological conditions, such as changes in groundwater levels and local hydrochemical variations, can vary significantly. The increase in heavy metal concentration represents a significant risk to living organisms, both flora and fauna, and can even be lethal (Béjaoui *et al.*, 2016; Doumas *et al.*, 2018).

CONCLUSIONS

This study employed Electrical Resistivity Imaging (ERI) to investigate the internal structure of the abandoned tailings ponds in the Hiendelaencina mining district and to evaluate the spatial and temporal variations in water content. Several key conclusions can be drawn from the findings:

- The resistivity profiles provided a clear picture of the geometry and thickness of the tailings and showed that they were deposited directly onto the pre-existing horizontal topographic surface. The results indicated that the tailings reached maximum thicknesses of 15m in the North pond and 10m in the South pond.

- Temporal variations in resistivity between autumn of 2020 and spring 2021 allowed us to infer changes in water content. The water content in the tailings increased significantly after the spring rains, while the fractured metamorphic basement and underlying sedimentary Cenozoic materials showed a marked increase in water saturation.

- The data indicate the presence of water infiltration from the tailings into the underlying sedimentary and metamorphic rocks. This infiltration was observed both laterally and vertically, and was particularly pronounced in areas of fractured metamorphic rocks. The findings demonstrate that the tailings ponds are not impermeable, with water percolating into deeper layers, potentially carrying dissolved contaminants.

- The observed water infiltration poses potential environmental risks, particularly the transfer of pollutants from the tailings into the subsurface and surrounding groundwater systems. Given the permeability of the fractured zones, these findings highlight the need for further monitoring and potential mitigation measures to prevent groundwater contamination.

This study acknowledges that no direct soil moisture measurements were available to calibrate ERI-derived water content values. As a result, it should be regarded as qualitative indicators of relative changes rather than absolute values. Nevertheless, the use of ERI has proven to be an effective tool for characterizing the internal structure of mine tailings and monitoring changes in water content over time. The methodology described here provides a robust approach for assessing the environmental impact of abandoned mining sites and contributes to a broader understanding of subsurface water dynamics in contaminated areas.

ACKNOWLEDGMENTS

This research was funded by the Comunidad de Madrid and Universidad Rey Juan Carlos (projects M2167 and M2373). The authors thank the "Hiendelaencina Silver Mining Interpretation Center" for the logistical support provided during the development of this work. The authors would like to thank the editors and the two anonymous reviewers for their valuable suggestions, which significantly improved the quality of the manuscript.

REFERENCES

AEMET, 2022. Agencia Estatal de Meteorología-AEMET. Gobierno de España. URL. Last accessed: 09 June 2023 . Website: http://www.aemet.es/es/portada

Alengebawy, A., Abdelkhalek, S.T., Qureshi, S.R., Wang, M.Q., 2021. Heavy Metals and Pesticides Toxicity in Agricultural Soil and Plants: Ecological Risks and Human Health Implications. Toxics, 25(9), 42. DOI: 10.3390/toxics9030042

Archie, G.E., 1942. The electrical resistivity log as an aid in determining some reservoir characteristics. Petroleum Technology, 5(1), 1-8.

Bai, G., Sun, Q., Geng, J., Wang, S., Jing, X., 2022. Resistivity of granite and sandstone varies with frequency and water saturation. Geomechanics and Geophysics for Geo-energy and Geo-Resources, 8, 198. DOI: 10.1007/s40948-022-00503-1

Béjaoui, I, Kolsi-Benzina, N., Sappin-Didier, V., Munoz, M., 2016. Health risk assessment in calcareous agricultural soils contaminated by metallic mining activity under mediterranean climate. CLEAN- Soil, Air, Water, 44, 1385-1395.

Belén, A., De Pablo, M., 2016. Calidad escénica de los paisajes de Hiendelaencina (Guadalajara, España). De Re Metallica

(Madrid): Revista de La Sociedad Española Para La Defensa Del Patrimonio Geológico y Minero, 43-53.

Bernard J., 2003. Short note on the depth of investigation of electrical methods. Orleans (France), IRIS Instruments, 8pp.

Brillante, L., Mathieu, O., Bois, B., van Leeuwen, C., Lévêque, J., 2015. The use of soil electrical resistivity to monitor plant and soil water relationships in vineyards. Soil, 1, 273-286. Last accessed: Website: https://doi.org/10.5194/soil-1-273-2015, 2015.

Bussian, A.E., 1983. Electrical conductance in a porous medium. Geophysics, 48, 1258-1268. DOI: https://doi.org/10.1190/1.1441549.

Cacciuttolo, C., Cano, D., Custodio., M., 2023. Socio-Environmental Risks Linked with Mine Tailings Chemical Composition: Promoting Responsible and Safe Mine Tailings Management Considering Copper and Gold Mining Experiences from Chile and Peru. Toxics 11(5), 462. DOI: https://doi.org/10.3390/toxics11050462

Calvo, M., Sevillano, E., 1992. Famous Mineral Localities: Hiendelaencina, Spain. Mineralogical Record, 23, 241-249.

Chambers, J.E., Meldrum, P.I., Gunn, D.A., Wilkinson, P.B., West, J.M., Kuras, O., 2010., 3D geological mapping of buried valley networks: application of surface-based and airborne geophysical methods at the Ness of Quoys wind farm, Orkney. Near Surface Geophysics, 8(6), 557-568.

Concha, A., Oyarzun, R., Lunar, R., Sierra, J., Doblas, M., Lillo, J., 1992. The Hiendelaencina epithermal silver-base metal district, Central Spain: Tectonic and mineralizing processes. Mineralium Deposita, 27, 83-89.

Daily, W., Ramirez, A., Owen, E., 1992. Imaging of environmental and geotechnical problems using electrical resistivity tomography. Geophysics, 57(6), 747-753.

De Araújo, S.N., Ramos, S.J., Martins, G.C., Teixeira, R.A., de Souza, E.S., Sahoo, P.K., Fernandes, A.R., Gastauer, M., Caldeira, C.F., Souza-Filho, P.W.M., Dall'Agnol, R., 2022. Copper mining in the eastern Amazon: An environmental perspective on potentially toxic elements. Environmental, Geochemistry and Health, 44, 1767-1781.

De Jong, S.M., Addink, E.A., Doerr, S.H., van der Meij, W.M., Sterk, G., 2020. Monitoring soil moisture changes using time-lapse electrical resistivity tomography in a field-scale rainfall experiment. Journal of Hydrology, 590, 125393. DOI: https://doi.org/10.1016/j.jhydrol.2020.125393.

De Lima, O.A.L., Sharma, M.M., 1990. A grain conductivity approach to shaly sandstones. Geophysics, 55, 1347-1356. DOI: https://doi.org/10.1190/1.1442782.

De Pablo, M., de Pablo, J., Paniego, M., 2013. Proyecto De Recuperación Del Entorno De La Mina De Plata San Carlos (Hiendelaencina, Guadalajara). De Re Metallica (Madrid): Revista de La Sociedad Española Para La Defensa Del Patrimonio Geológico y Minero, 53-64

Dietrich, S., Weinzettel, P.A., Varni, M., 2014. Infiltration and drainage analysis in a heterogeneous soil by electrical resistivity tomography. Soil Science Society of American Journal, 78(4), 1153-1167.

Dimech, A., Cheng, L., Chouteau, M., Chambers, J., Uhlemann, S., Wilkinson, P., Meldrum, P., Mary, B., Fabien-Ouellet, G., Isabelle, A., 2022. A Review on Applications of Time-Lapse Electrical Resistivity Tomography Over the Last 30 Years: Perspectives for Mining Waste Monitoring. Surveys in Geophysics, 43, 1699-1759. DOI: https://doi.org/10.1007/s10712-022-09731-2

Dimech, A., Isabelle, A., Sylvain, K., Liu, Ch., Cheng, L., Bussière, B., Chouteau, M., Fabien-Ouellet, G., Bérubé, Ch., Wilkinson, P., Meldrum, Ph., Chambers, J., 2023. A multiscale accuracy assessment of moisture content predictions using time-lapse electrical resistivity tomography in mine tailings. Scientific Reports, 13, 20922. DOI: https://doi.org/10.1038/s41598-023-48100-w

Dold, B., 2014. Evolution of acid mine drainage formation in sulphidic mine tailings. Minerals, 4, 621-641.

Doumas, P., Munoz, M., Banni, M., Becerra, S, Bruneel, O., Casiot, C., Cleyet-Marel, J.C., Gardon, J., Noack, Y., Sappin-Didier, V., 2018. Polymetallic pollution from abandoned mines in Mediterranean regions: a multidisciplinary approach to environmental risks. Regional Environmental Change, 18, 677-692. DOI: https://doi.org/10.1007/s10113-016-0939-x.

Dudka, S., Adriano, D.C., 1997. Environmental impacts of metal ore mining and processing: a review. Journal of environmental quality, 26(3), 590-602.

ESDAT, 2009. Soil Remediation Circular. Last accessed: Website: https://www.esdat.net/Environmental%20Standards/Dutch/ENGELSE%20versie%20circulaire%20Bodemsanering%202009.pdf

García García, C., 2004. Impacto y riesgo ambiental de los residuos minero-metalúrgicos de la sierra de Cartagena-La Unión (Murcia, España). PhD Thesis. Cartagena, Universidad Politécnica de Cartagena, 460pp.

Garré, S., Javaux, M., Vanderborght, J., Pagès, L., Vereecken, H., 2011. Three-Dimensional Electrical Resistivity Tomography to Monitor Root Zone Water Dynamics. Vadose Zone Journal, 10, 412-424. DOI: https://doi.org/10.2136/vzj2010.0079

Gómez-Ortiz, D., Martín-Velázquez, S., Martín-Crespo, T., De Ignacio-San José, C., Lillo, J., 2010. Application of electrical resistivity tomography to the environmental characterization of abandoned massive sulphide mine ponds (Iberian Pyrite Belt, SW Spain). Near Surface Geophysics, 8, 65-74.

González, O., 2011. Impacto ambiental de las áreas de minería metálica: Aplicación de metodologías analíticas no destructivas al análisis geoquímico. PhD Thesis. Barcelona, Universidad Autónoma de Barcelona, 388pp.

Grellier, S., Robain, H., Bellier, G., Skhiri, N., 2006. Influence of temperature on the electrical conductivity of leachate from municipal solid waste. Journal of Hazardous Materials, 137(1), 612-617. DOI: https://doi:10.1016/j.jhazmat.2006.02.049

Hayley, K., Bentley, L.R., Gharibi, M., Nightingale, M., 2007. Low temperature dependence of electrical resistivity: Implications for near surface geophysical monitoring. Geophysical Research Letters, 34(18),pp. DOI: https://doi.org/10.1029/2007GL031124

Hermans, T., Nguyen, F., Robert, T., Revil, A., Lambot, S., 2014. Electrical resistivity tomography monitoring of a controlled infiltration experiment. Hydrology and Earth System Sciences, 18, 493-504. DOI: https://doi.org/10.5194/hess-18-493-2014

Ibraheem, I.M., Tezkan, B., Bergers, R., 2021. Integrated Interpretation of Magnetic and ERT Data to Characterize a Landfill in the North-West of Cologne, Germany. Pure and Applied Geophysics, 178, 2127-2148. DOI: https://doi.org/10.1007/s00024-021-02750-x

IGME, Instituto Geológico y Minero de España, 1972. Informe sobre trabajos de investigación minera y sus resultados en los filones de la zona de Hiendelaencina (Guadalajara). Madrid, IGME.

IGME, Instituto Geológico y Minero de España, 1999a. Información sobre la balsa 0460-3-0001. Last accessed: Website: http://info.igme.es/balsas/InfoBalsa.aspx?id=0460-3-0001

IGME, Instituto Geológico y Minero de España, 1999b. Información sobre la balsa 0460-3-0002. Last accessed: Website: http://info.igme.es/balsas/InfoBalsa.aspx?id=0460-3-0002

Jarsjö, J., Chalov, S.R., Pietroń, J., Alekseenko, A.V., Thorslund, J., 2017., Patterns of soil contamination, erosion and river loading of metals in a gold mining region of northern Mongolia. Regional Environmental Change, 17, 1991-2005.

Jayawickreme, D.H., Van Dam, R.L., Hyndman, D.W., 2010. Hydrological consequences of land-cover change: Quantifying the influence of plants on soil moisture with time-lapse electrical resistivity. Geophysics, 75(4), WA43-WA50.

Jiang, Z., Fu, J., Li, G., Mao, Z., Zhao, P., 2021. Using resistivity data to study the waterflooding process: a case study in tight sandstone reservoirs of the Ordos Basin, China. Geophysics, 86(2), B55-B65. DOI: https://doi.org/10.1190/geo2020-0401.1

Jörg GöttlicherKirkby, A., Heinson, G., 2017. Three-dimensional resistor network modeling of the resistivity and permeability of fractured rocks. Journal of Geophysical Research, Solid Earth, 122, 2653-2669. DOI: https://doi.org/10.1002/2016JB013854

Kossoff, D., Dubbin, W.E., Alfredsson, M., Edwards, S.J., Macklin, M.G., Hudson-Edwards, K.A., 2014. Mine tailings dams: Characteristics, failure, environmental impacts, and remediation. Applied geochemistry, 51, 229-245.

Köppen, W., 1931. Grundriss der Klimakunde. Berlín, De Grutier, 388pp.

Kučerová, G., Majzlan, J., Lalinská-Voleková, B., Radková, A., Bačík, P., Michňová, J., Šottník, P., Jurkovič, L., Klimko, T., Steininger, R., 2014. Mineralogy of neutral mine drainage in the tailings or siderite-Cu ores in eastern Slovakia. The Canadian Mineralogist, 52, 779-798. DOI: https://doi.org/10.3749/canmin.1400020

Lee, H., Lee, J.W., Oh, T.M., 2021. Permeability evaluation for artificial single rock fracture according to geometric aperture variation using electrical resistivity. Journal of Rock Mechanics and Geotechnical Engineering, 13, 787-797. DOI: https://doi.org/10.1016/j.jrmge.2021.04.003

Lewis, A.E., 2010. Hydrometallurgy Review of metal sulphide precipitation. Hydrometallurgy, 104(2), 222-234.

Lindsay, M.B.J., Moncur, M.C., Bain, J.G., Jambor, J.L., Ptacek, C.J., Blowes, D.W., 2015. Geochemical and mineralogical aspects of sulfide mine tailings. Applied Geochemistry, 157-177.

Liu, B., Sun, Y., Wang, B., Han, Y., Zhang, R., Wang, J., 2020. Effect of water content on mechanical and electrical characteristics of the water-rich sandstone during freezing. Environmental Earth Sciences, 79, 236-314. DOI: https://doi.org/10.1007/s12665-020-08991-8

Loke, M.H., 2011. Tutorial: 2-D and 3-D electrical imaging surveys. In: Hydrogeophysics, Springer, 93-130.

Loke, M.H., Chambers, J.E., Rucker, D.F., Kuras, O., Wilkinson, P.B., 2013., Recent developments in the direct-current geoelectrical imaging method. Journal of Applied Geophysics, 95, 135-156.

López Gómez, A., 1969. El distrito minero de Hiendelaencina (Guadalajara). Cuadernos de Geografía, 6, 211-250.

Lysdahll, A.K., Bazinl, S., Christensen, C., Ahrens, S., Gunther, T., Pfaffhuberl, 2017. A Comparison between 2D and 3D ERT inversion for engineering site investigations – a case study from Oslo Harbour. Near Surface Geophysics, 15, 201-209. DOI: https://doi.org/10.3997/1873-0604.2016052

Ma, R., Li, G., Zhang, H., Wang, X., Liu, Y. 2011. Temperature effect on electrical resistivity of soils. Engineering Geology, 117(1-2), 52-57. DOI: https://doi.org/10.1016/j.enggeo.2010.10.011

Martín-Crespo, T., de Ignacio, C., Gómez-Ortiz, D., Martín-Velázquez, S., Lillo, J., 2010. Monitoring study of the mine pond reclamation of Mina Concepción, Iberian Pyrite Belt (Spain). Enviromental Earth Sciences, 59, 1275-1284. DOI: https://doi.org/10.1007/s12665-009-0115-4

Martín-Crespo, T., Gómez-Ortiz, D., Martín-Velázquez, S., 2019. Geoenvironmental characterization of sulfide mine tailings. In: Mazadiego, L.F., de Miguel García, E., Barrio-Parra, F., Izquierdo-Díaz, M. (eds.). Applied Geochemistry with Case Studies on Geological Formations, Exploration Techniques and Environmental Issues. IntechOpen, 85-109.

Martín-Crespo, T., Gomez-Ortiz, D., Pryimak, V., Martín-Velázquez, S., Rodríguez-Santalla, I., Ropero-Szymañska, N., de Ignacio, C., 2023. Quantification of Pollutants in Mining Ponds Using a Combination of LiDAR and Geochemical Methods. Mining District of Hiendelaencina, Guadalajara (Spain). Remote Sensing, 15(5),1423. DOI: https://doi.org/10.3390/rs15051423

Martín-Velázquez, S., Rodríguez-Santalla, I., Ropero-Szymañska, N., Gómez-Ortiz, D., Martín-Crespo, T., De Ignacio, C., 2022. Geomorphological Mapping and Erosion of Abandoned Tailings in the Hiendelaencina Mining District (Spain) from Aerial Imagery and LiDAR Data. Remote Sensing, 14, 4617.

Martínez-Frías, J., 1992. The Hiendelaencina mining district (Guadalajara, Spain). Mineralium Deposita, 27(3), 206-212.

Martínez-López, S., Martínez-Sánchez, M.J., Pérez-Sirvent, C., 2021. Do Old Mining Areas Represent an Environmental Problem and Health Risk? A Critical Discussion through a Particular Case. Minerals, 11, 594.

Martínez-Pagán, P., Gómez-Ortiz, D., Martín-Crespo, T., Martín-Velázquez, S., Martínez-Segura, M., 2021. Electrical Resistivity Imaging Applied to Tailings Ponds: An Overview.

Mine Water Environment, 40, 285-297. DOI: https://doi.org/10.1007/s10230-020-00741-3

Meza-Figueroa, D., Maier, R.M., De la O-Villanueva, M., Gómez-Alvarez, A., Moreno-Zazaueta, A., Rivera, J., Campillo, A., Grandlic, C.J., Anaya, R., Palafox-Reyes, J., 2009. The impact of unconfined mine tailings in residential areas from a mining town in a semi-arid environment: Nacozari, Sonora, Mexico. Chemosphere, 77, 140-147.

Mohamad, A.M., Hamada, G.M., 2017. Determination techniques of Archie's parameters: a, m and n in heterogeneous reservoirs. Journal of Geophysics and Engineering, 14(6), 1358-1367. DOI: https://doi.org/10.1088/1742-2140/aa805c

Mollehuara Canales, R.C., Kozlovskaya, E., Lunkka, J.P., Guan, H., Banks, E., Moisio, K., 2020. Geoelectric interpretation of petrophysical and hydrogeological parameters in reclaimed mine tailings areas. Journal of Applied Geophysics, 181, 104139. DOI: https://doi.org/10.1016/j.jappgeo.2020.104139.

Neyamadpour, A., 2019. 3D electrical resistivity tomography as an aid in investigating gravimetric water content and shear strength parameters. Environmental Earth Sciences, 78(19), 1-14.

Olías, M., Nieto, J.M., Pérez-López, R., Cánovas, C.R., Macías, F., Sarmiento, A.M., Galván, L., 2016. Controls on acid mine water composition from the Iberian Pyrite Belt (SW Spain). Catena, 137, 12-23.

Pashkevich, M.A., 2017. Classification and environmental impact of mine dumps. In: Bech, J., Bini, C., Pashkevich, M.A. (eds.). Assessment, Restoration and Reclamation of Mining Influenced Soils. Academic Press, 1-32.

Portero, J.M., Pérez González, A., Díaz Molina, M., Gallardo, M.J., González Lodeiro, F., Aguilar, M.J., Leal, C., 1982. Mapa Geológico Nacional Serie MAGNA escala 1:50.000. Hoja 460 (Hiendelaencina). Madrid, Instituto Geologico y Minero de España (IGME), Edición 1990.

Rao, S., Lesparre, N., Flores, A., Wagner, F., Kemna, A., Javaux, M., 2020. Imaging plant responses to water deficit using electrical resistivity tomography. Plant and Soil, 454, DOI: https://doi.org/10.1007/s11104-020-04653-7.

Rekapalli, R., Sarma, V.S., Phukon, P., 2015. Direct resistivity measurements of core sample using a portable in-situ DC resistivity meter in comparison with HERT data. Journal of the Geological Society of India, 86, 211-214. DOI: https://doi.org/10.1007/s12594-015-0300-x

Revil, A., Glover, P.W.J., 1998. Nature of surface electrical conductivity in natural sands, sandstones and clays. Geophysical Research Letters, 25, 691-694.

Revil, A., Soueid Ahmed, A., Matthai, S., 2018. Transport of water and ions in partially water-saturated porous media. Part 3. Electrical conductivity. Advances in Water Resources, 121, 97-111. DOI: https://doi.org/10.1016/j.advwatres.2018.08.007.

Reynolds, J.M., 2011. An Introduction to Applied and Environmental Geophysics. Chichester (UK), Wiley-Blackwell, 712pp.

Rodríguez-Pacheco, R., Butlanska, J., Oliva-González, A.O., 2025. Geotechnical and Hydrogeological Zonation of Tailings Storage Facilities: Importance for Design, Construction, Operation, and Closure. Minerals, 15, 105. DOI: https://doi.org/10.3390/min15020105

Senger, K., Birchall, T., Betlem, P., Ogata, K., Ohm, S., Olaussen, S., Paulsen, R.S., 2021. Resistivity of reservoir sandstones and organic rich shales on the Barents Shelf: implications for interpreting CSEM data. Geoscience Frontiers, 12(6), 101063. DOI: https://doi.org/10.1016/j.gsf.2020.08.007.

Slater, L., Binley, A., 2003. The use of electrical imaging surveys to characterize preferential flow paths in soils. Journal of Hydrology, 272(1-4), 192-204.

Smith, K.S., 2007. Strategies to predict metal mobility in surficial mining environments. GSA Reviews in Engineering Geology, 17(03), 25-45.

Tso, C.H.M., Knappett, J., Odenwald, C., 2019. On the use of electrical resistivity imaging to estimate in-situ moisture content in unsaturated soils. Engineering Geology, 260, 105199. DOI: https://doi.org/10.1016/j.enggeo.2019.105199.

Vanella, D., Ramírez-Cuesta, J.M., Sacco, A., Longo-Minnolo, G., Luigi Cirelli, G., Consoli, S., 2021. Electrical resistivity imaging for monitoring soil water motion patterns under different drip irrigation scenarios. Irrigation Science, 39, 145-157. DOI: https://doi.org/10.1007/s00271-020-00699-8

Vásquez, K.Y., Orellana, S.A., Monsalve, S.M., Vergara, J.K., Zamora, C.S., Muñoz, D.V., Lillo, D.D.C., 2015. Exposure to fine particles by mine tailing and lung function effects in a panel of schoolchildren, Chañaral, Chile. Journal of Environmental Protection, 6(2), 118-128.

Waxman, M.H., Smits, L.J.M., 1968. Electrical conductivities in oil-bearing shaly sands. Society of Petroleum Engineers Journal, 8, 107-122. DOI: https://doi.org/10.2118/1863-A

Whitman, D., Yeboah-Forson, A., 2015. Electrical resistivity and porosity structure of the upper biscayne aquifer in miami-dade county, Florida. Journal of Hydrology, 531, 781-791. DOI: https://doi.org/10.1016/j.jhydrol.2015.10.049

Žibret, G., Gosar, M., Miler, M., Alijagić, J., 2018. Impacts of mining and smelting activities on environment and landscape degradation—Slovenian case studies. Land Degradation & Development, 29(12), 4457-4470.

Manuscript received May 2025;
revision accepted October 2025;
published Online December 2025.